

Advances in multifocal methods for imaging human brain activity

Thom Carney*^{ab}, Justin Ales^b, Stanley A. Klein^b

^a Neurometrics Institute, Oakland, CA

^b School of Optometry, Univ. of California at Berkeley, Berkeley, CA

ABSTRACT

The typical multifocal stimulus used in visual evoked potential (VEP) studies consists of about 60 checkerboard stimulus patches each independently contrast reversed according to an m-sequence. Cross correlation of the response (EEG, MEG, ERG, or fMRI) with the m-sequence results in a series of response kernels for each response channel and each stimulus patch. In the past the number and complexity of stimulus patches has been constrained by graphics hardware, namely the use of look-up-table (LUT) animation methods. To avoid such limitations we replaced the LUTs with true color graphic sprites to present arbitrary spatial patterns. To demonstrate the utility of the method we have recorded simultaneously from 192 cortically scaled stimulus patches each of which activate about 12mm² of cortex in area V1. Because of the sparseness of cortical folding, very small stimulus patches and robust estimation of dipole source orientation, the method opens a new window on precise spatio-temporal mapping of early visual areas. The use of sprites also enables multiplexing stimuli such that at each patch location multiple stimuli can be presented. We have presented patterns with different orientations (or spatial frequencies) at the same patch locations but independently temporally modulated, effectively doubling the number of stimulus patches, to explore cell population interactions at the same cortical locus. We have also measured nonlinear responses to adjacent pairs of patches, thereby getting an edge response that doubles the spatial sampling density to about 1.8 mm on cortex.

Keywords: multifocal, sprite, m-sequence, VEP, visual cortex, multi-pattern, brain imaging

1. INTRODUCTION

With the advent and proliferation of the multifocal m-sequence evoked potential method it has become routine to generate accurate detailed maps of retinal function for clinical assessment¹. More recently the technique has been successfully applied to later stages of visual processing, namely the early retinotopic areas of visual cortex². The technique provides a electrophysiological means of estimating cortical magnification³ and studying the M and P pathways in humans⁴. The multifocal method has spread to other response measures such as pupilometry⁵ and fMRI⁶ for demonstrating retinotopic responses. In general the methodological details are stable with occasional modifications to emphasize certain functionality such as increasing SNR⁷. To achieve our long term goals we have had to extend the standard method to include stimuli of increased complexity. The typical multi-focal cortically scaled dartboard stimulus consists of about 60 checkerboard stimulus patches each independently contrast reversed according to an m-sequence⁸. Cross correlation of the EEG signal with the m-sequence results in a series of response kernels for each electrode and each stimulus patch^{9,10,11}. The number and complexity of stimulus patches has been constrained by the standard method which utilized the LUT hardware of common PC graphic cards. Moreover, kernel overlap is also a problem to be considered in dense multi patch displays.

We have overcome these limitations by: a) replacing look-up-table animation with true color graphic sprites to present arbitrary spatial patterns, and b) a variety of time shift manipulations to limit kernel overlap. With these two modifications one can record simultaneously from hundreds of patches each activating areas in V1 of about 12 mm². It is anticipated that this extended multifocal VEP technique in combination with the sparseness of cortical folding as a uniqueness constraint will become an effective method for localizing signal sources in early visual areas having a

retinotopic organization. Moreover, using sprites it is now possible to multiplex stimuli such that at each patch location multiple stimuli can be presented to explore response linearity and local cell population interactions.

2. GENERAL METHODS

2.1 EEG recording

Ninety six active EEG recording electrodes were distributed over the scalp with a heavy weighting over the occipital pole as shown in figure 1. For some stimulus conditions, recordings were performed on successive days so care was taken applying the electrode cap at the same position across days. The EEG recording amplifiers were broad band with digital bandpass filtering of 2 to 30 Hz, applied offline. Each 16 bit m-sequence run was broken into 18, 1 minute recording segments with 1 second of segment overlap for combining segments during offline processing. The subject controlled the initiation of each recording segment allowing for brief rest periods between each segment. Besides the EEG signals, event channels recorded segment start and stop times along with the m-sequence state for patch 1. The event channels were used to co-register the digitally sampled EEG data with the stimulus presentation sequence. After combining segments and signal interpolation the sampling is 9 samples per m-sequence step (540 Hz).

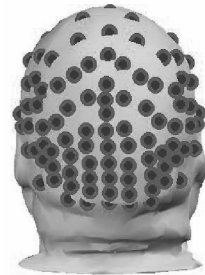


Figure 1 - 96 electrodes

2.2 Multifocal m-sequence method

The multifocal technique is related to white noise analysis. Every individual patch is modulated with a temporally white sequence. If the input to a system is white it is simply a matter of cross correlating the input with the output to derive the response kernels for the system. In addition, for any given sequence length, there are many choices of values that will result in white statistics. The standard multifocal technique uses maximum length, or m-sequences. In addition to other properties that make them particular well suited for non-linear systems analysis, these sequences have autocorrelation functions that are perfect impulses. In order to study the response due to multiple stimuli simultaneously each separate stimulus is driven with a temporally shifted sequence. This will result in the impulse response having a delay when cross correlated with the originally, non-delayed, sequence. Then to match the response with the individual stimuli it is simply a matter of looking at the time window with the appropriate delay. In this way multifocal stimulation allows for an efficient way to combine many different stimuli in one experiment¹¹.

2.3 Stimulus characterization

Subjects view the display screen from within a dark sound attenuating chamber. Stimuli were presented on a 60 Hz video display (1024 x 768 pixels) and viewed from a distance of 109 cm (1.14 min square pixels). Luminance gamma correcting tables linearized the final display luminance. The stimuli were 15 deg. diameter dartboard shaped patterns consisting of from 4 – 24 spokes and from 3 – 8 concentric cortically scaled rings⁸ for up to a total of 192 independent stimulus patches. The surrounding screen area and the central 0.5 deg diameter patch of the stimulus remained at the display mean luminance, 8.4 cd/m². A small bright fixation 'X' was placed at the center of the display which the subject used to maintain fixation during each of the 1 min recording segments.

Advanced sprite graphics multi-pattern multifocal method: The WinVis (W4M) psychophysical and physiological testing toolbox (www.neurometrics.com/winvis) was used to present multi-state sprite objects to avoid the limitations of both the LUT animation and the prerecorded movie method of m-sequence stimulus temporal modulation. Using a 16 bit m-sequence with the stimulus updated on every video frame (60 Hz) results in a 65535 ($2^{16} - 1$) video frame sequence. While it is possible to pre-compute a movie of the stimulus sequence it is generally not a practical approach in that it is time consuming and will likely require image compression for the sequence to fit in memory, even after dissecting the typical 20 minute sequence into 1 minute segments ($768*1024*3600(\text{frames}) \sim 2.8$ gigabytes). It is critical that the display system be accurately synchronized and avoids frame drops which are the bane of multifocal stimulation. To alleviate the memory demands the standard multifocal method uses hardware LUT animation which only requires 768 bytes (standard 256x3 LUT) to change the stimulus pattern on every video frame. However, you are then limited to 128 checkerboard (two intensity level) stimulus patches using the standard graphics card hardware LUT. Some 20-30 years ago the early PCs made use of special hardware chips to implement sprite graphics whereby small images could be easily placed at different positions on the video screen on a frame by frame basis to create interesting

animations (games) without requiring excessive memory. Today's computer graphics cards generally include some form of sprite graphics in hardware, however, computers are now fast enough that sprites can also be implemented in software to create stunning effects. Our typical sprite based multifocal stimulus requires around 1.5 megabytes of data transfer per video frame plus significant sprite transparency logic, a significant increase from LUT based methods but not particularly taxing for modern desktop/laptop CPUs. The WinVis (W4M) toolbox (www.neurometrics.com/winvis) has built-in software based sprite graphics support and was consequently used to present multi-state sprite objects to avoid the limitations of both LUT animation and precomputed m-sequence movies.

The sprite based method not only extends well beyond the 128 patch limit of LUT methods it also enables stimulus patches to use the full grayscale (color) range within each patch. With standard LUT methods each doubling of the number of intra-patch intensity levels halves the number of available patches. For example, only 8 independent stimulus patches are possible if each stimulus patch requires a modest 16 intensity levels. Sprites avoid the tradeoff between patch count and available intensity levels, each patch can span the range of intensity levels the graphics card supports independent of the number of sprites (stimulus patches) being presented. Finally, another main advance derived from using sprite graphics is the ability to use multiple independently modulated stimulus patterns within a single stimulus patch. The details of this innovation and a specific example are described in the orthogonal orientation multi-pattern stimulus section.

Dense 192 patch stimulus: Our primary purpose for using a stimulus with such small stimulus patches is to enable us to identify the signal sources in early visual areas. With small patches correspondingly small areas of retinotopically organized visual cortex (V1, V2 and V3) are activated. Adjacent stimulus patches activate adjacent cortical patches. The specific scalp topography of the signal resulting from a particular patch of cortical activation reflects the local cortical surface normal. Given the extensive cortical folding, as you move from patch to patch in stimulus space the response topography should change according to the summed changes in the local cortical surface normals for early visual areas. The sequence of changes will enable us to ultimately identify the source locations in the early visual areas.

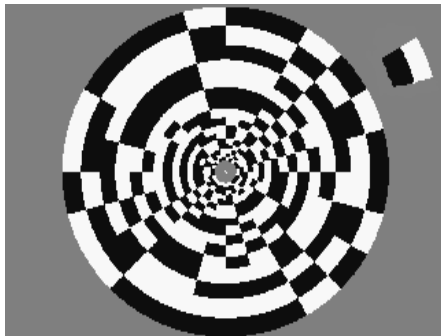


Figure 2 - One frame of 192 patch stimulus

This 192 sprite stimulus patch configuration (figure 2) consists of 8 concentric rings of 24 patches each. Each patch has two checks (one black and one white) in the radial direction and a single check in tangential direction. A single patch for the outer ring is shown in the upper right of figure 2. The size of each patch in the radial direction is scaled according to estimates of cortical magnification whereby the more eccentric the ring the larger the patch⁸. The stimulus is scaled in this manner to provide approximately equal areas of cortical activation irrespective of stimulus eccentricity. We estimate the cortical patch size in area V1 to be approximately 3.5 mm in the stimulus tangential and radial directions¹². An example of one video frame of this stimulus is shown figure 2. Note each

patch consists of one cycle of a tangential squarewave grating which is counterphase flickered according to a binary m-sequence. The temporal modulation of each stimulus patches is based on time shifted versions of the same m-sequence.

A major concern in multi-focal stimulation is to avoid response kernel overlap. By searching for m-sequence seeds that maximize relevant kernel separation, judicious padding of delays in each stimulus ring and placement of multiple stimuli with reasonably short ISIs we optimized the final response kernel placement so that a larger than expected number of stimuli could be superimposed without kernel overlap.

Segmented grayscale face stimulus: As a simple proof of concept we subdivided an image of Einstein into a 32 patch dartboard pattern, 4 rings by 8 patches/ring (figure 3). Each patch alternated between the part of the Einstein image and a mean luminance background according to a 16 bit m-sequence. This stimulus demonstrates that any arbitrary gray scale image can be used in sprite based multi-focal stimulation. The traditional LUT based multifocal method only requires about 768 bytes uploaded to the graphic card on every video frame. For sprite graphics, assuming 50% of the area of each sprite pattern includes a transparent area which overlaps with nearby sprites, every video frame requires about 1.2 megabytes (1024*768*1.5) of image data transferred to the video card on every video

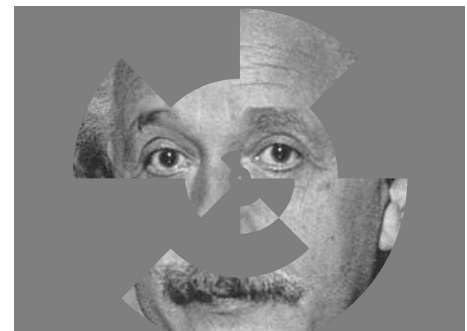


Figure 3 - Arbitrary gray scale patches

frame. Besides the raw data throughput, the computational demand of the transparency logic is significant so only relatively fast desktop computers can keep up at the full video frame rate. The stimuli described in this document are all presented in an 8 bit grayscale video mode but 32 bit true color video modes can also be used to incorporate the full color gamut in multifocal stimuli. However, true color video modes demand about 3 times as many CPU cycles and consequently not all systems are able to complete the screen update without occasional frame drops.

Orthogonal orientation multi-pattern multifocal stimulus: A special feature of the sprite multifocal method is the ability to present multiple stimulus patterns at the same patch location within the same run. Normally only a single pattern

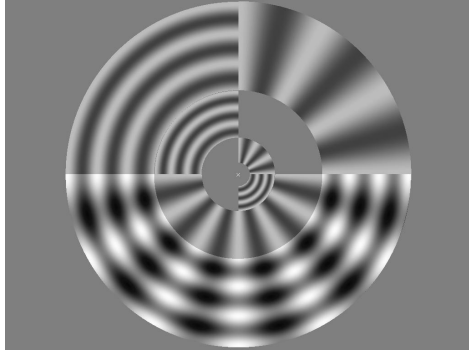


Figure 4 - Multi-pattern stimulus

within the patch area is modulated between two states according to an m-sequence to elicit an evoked cortical response. As stated earlier, every stimulus patch is modulated by the same m-sequence but with different start and stop points, or equivalently a temporally shifted m-sequence. Suppose one is interested in sampling two underlying cell populations at the same spatial location. For example consider orientation tuned cortical neurons, with different cell populations responsive to horizontal versus vertical orientations. A multifocal VEP experiment with patch grating patterns oriented vertically will elicit signals from cells responsive to vertical (except for patch edge effects) and visa versa for an experiment using horizontally oriented grating patterns. The efficiency of the standard multifocal method derives from being able to extract the VEP associated with a particular stimulus patch in the presence of many other stimulus patches being simultaneously modulated. We can extend this

efficiency to within a patch by simultaneously presenting multiple patterns each also modulated by the same m-sequence but with different time shifts. So in the case of vertical and horizontal grating patterns each counterphase pattern is modulated by an m-sequence and presented at the same location, yielding a total of four unique patterns at each patch (V, H, V+H, and O, where V & H are vertical and horizontal patterns respectively and O is mean luminance). In general, the number of unique stimuli or sprites required for each patch position is 2^N , where N is the number of patterns. In terms of unique stimuli limitations, since the displayed sprite on any individual video frame is limited to 100% contrast the individual patterns are limited in maximum contrast. For example a patch with 4 different patterns of equal contrast, each pattern is limited to 25% contrast which can reduce the efficiency of the method depending on the contrast response function of the responding cells. Finally, it would also be possible to use different sized patterns such that one pattern would extend over several smaller stimulus patches. This particular implementation of a multi-pattern multi-focal stimulus would be more difficult to create with $P2^N$ sprites required, where P is the number of patches the larger pattern extends over.

The multi-pattern multifocal example shown in figure 4 is one of three types of stimuli for which we compared the VEP's. The three stimulus types are: 1) a radial grating single-pattern multifocal stimulus, 2) a tangential grating single-pattern multifocal stimulus, and 3) the new tangent plus radial grating multi-pattern multifocal stimulus. Each stimulus contained 24 patches, 3 rings of 4 patches each, and spanned 15 degrees of visual angle. Both the tangent and radial grating component frequencies were 3 cycles/patch. Each grating component contrast was 49% (Michelson) such that the multi-pattern stimulus peak to peak contrast reached 98%. Figure 4 shows one video frame of the multi-pattern stimulus. Note that the multi-pattern stimulus contains all four patch states, mean luminance, tangent grating, radial grating and tangent plus radial grating. Four 16-bit m-sequence runs for each of the single-pattern conditions and seven 16-bit runs of the multi-pattern stimuli were performed. The extracted first order kernels were averaged within each stimulus condition.

To summarize, there were three experimental conditions. Condition one consisted of tangential gratings, much like that of the previous section except here the grating are luminance sinewaves rather than square wave patterns and the pattern changed from mean luminance field to a sinewave grating rather than counterphase flicker as in the previous section. Condition two was the same as condition one except the grating were radial gratings. Condition three consisted of same stimuli from conditions one and two but added and presented together.

3. RESULTS

3.1 Sparse cortical folding and dense visual field sampling – 1.8 mm cortical sampling

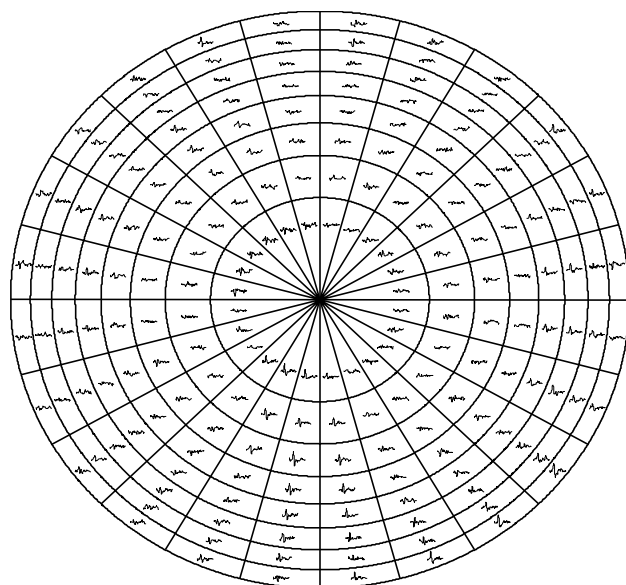


Figure 5 - Response to each of 192 patches

Early visual areas have close spatial proximity, a problem exacerbated by the extensive folding of the cortical sheet. VEP imaging methods are famous for their high temporal and poor spatial resolution. This is partly a result of dipole source analysis being unable to separate close sources in the presence of noise and poor head models. Many researchers have been applying physiological and anatomical cortical constraints to improve the solutions with some degree of success. Our latest approach is to use the sparseness of cortical folding and the robustness of the dipole orientations coming from dipole source analysis to identify source locations. With very small patches of cortical activation such as expected for the 192 patch stimulus, the equivalent dipole model is a good approximation with its orientation normal to the local cortical surface. While accurate dipole localization in the brain is problematic, the scalp voltage distribution strongly constrains the source orientation. An abrupt change in source orientation, as occurs for adjacent stimulus patches when the corresponding cortical patch of activation moves around a cortical fold, will result in a dramatic change in the scalp topography. The sparseness of cortical folding is

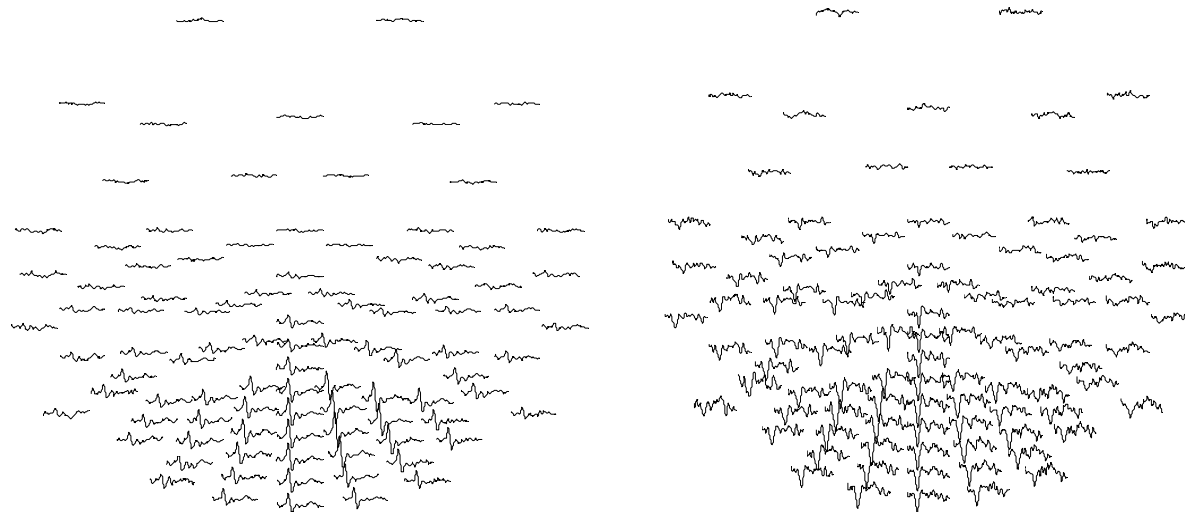


Figure 6 – a) patch 11, self kernel and b) patch 11/12 cross kernel responses

important for separating source locations in different visual areas; a change of source orientation in one area is not likely to coincide with a change in another visual area. Moreover, the multifocal method seems to limit activation to early retinotopic visual areas where receptive fields are small in size. Figure 5 shows the second-order response kernel for all the 192 patches from an electrode located at the posterior pole just to the right of the midline. At this size although details are hard to observe in the temporal waveforms; a VEP is evident for most stimulus patch locations. Figure 6a

(left side) shows the responses across the 96 electrodes for a single stimulus patch, the outer ring at 5 o'clock position. As expected the response focus was over the occipital pole and slightly stronger over the right hemisphere. One of the features of the multifocal method is the ability to extract kernels that reflect response interactions. For example, the cross kernel for adjacent patches along a ring reflect the response to the appearance and disappearance of an edge between adjacent patches. In the single video frame of figure 2 you can see regions that extend along the ring where patches are in the same state so patch borders are absent while in other regions you can easily discern the location of adjacent patches by the presence of an edge. The appearance and disappearance of the edge evokes a local response which may result from a local orientation change. When the edge is absent the local orientation is along the ring, however when the edge appears a local change of orientation (~45deg) would evoke a response in cells responsive to this orientation. Figure 6b, (right side) show the cross kernels between patch 11 and patch 12 along the outer ring. The cross kernel is weaker, perhaps reflecting a smaller more focal responding pool of neurons. The temporal response shape looks a little different which may due to changes in the relative activation of different visual areas, the effect of cortical topography changes between two patches or just the impact of reduced signal to noise. Interestingly, no significant cross kernel was evident between patches and rings going in the radial direction where the local patch edge orientation change was not present.

Singular value decomposition (SVD) was used to reduce the dimensionality of this large data set to help isolate response components associated with particular visual areas. Each VEP kernel is a function of electrode, patch and time, $V(e,p,t)$. Using SVD the data was decomposed into the sum of products of time dependent T_c and time independent E_c components:

$$V(e,p,t) = \sum E_c(e,p) T_c(t) \tag{1}$$

where E_c is the scalp weighting for each component and T_c is the temporal response for each component. It has been suggested that the first time component, that is the component that accounts for most of the variance during the signal window, is the time function of for area V1¹³. While this seems reasonable from considerations of response topography and the relative size of V1 compared to other areas, we assume the true V1 response is probably dominated by component 1 but includes some fraction of component 2. A strategy for connecting the orthogonal SVD component to

the true underlying sources is described in a later section. Figure 7 shows the variance the accounted for by the first 10 of a total of 192 components for both the self reversal kernels (counterphase patches) and the cross kernels. The first two components of the self kernels account for about 75% of the variance for the temporal window shown in figure 8. By comparison the first two cross kernel components only account for about 50% of the variance during the signal period, which reflects the lower signal to noise evident in figure 6. The left panel of Figure 8 shows the first two time functions (eigenvectors) for the 192 patch self kernels. The two components probably reflect the response of the cortical areas V1 and V2, the areas with the largest cortical representation. The right panel of Figure 8 shows the same SVD analysis applied to the

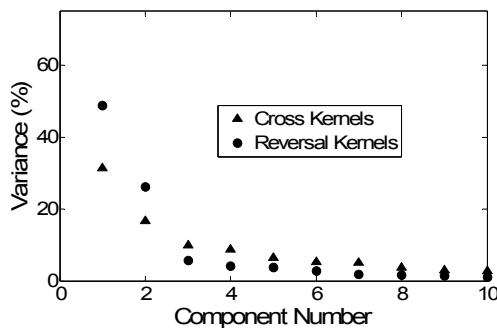


Figure 7 – Variance accounted for by components

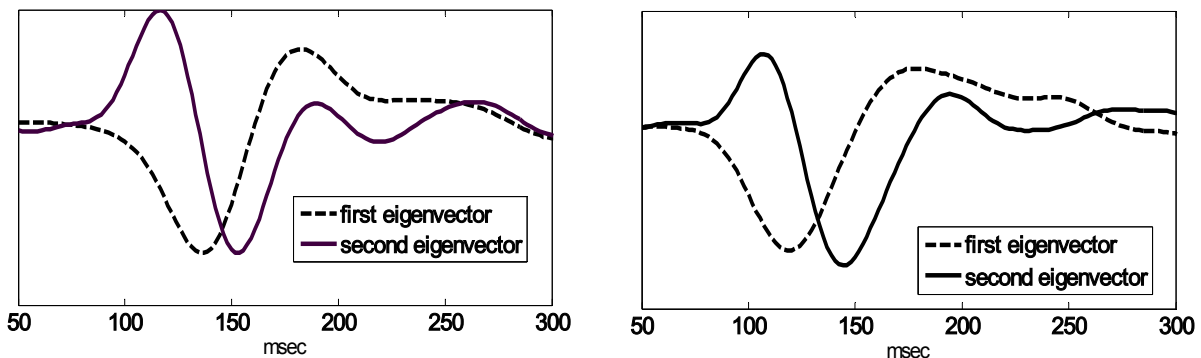


Figure 8 – a) First two temporal components for the self kernels b) same two components for the cross kernels

adjacent patch cross kernel data. The fact that the first two time components are very similar to the two components from the self kernels likely reflects activation of the same cortical areas.

As described, SVD analysis also provides the time independent weighting on each electrode for each patch location. Figure 9 shows the individual scalp topography electrode weightings for each of the 192 stimulus patches. The bottom row is the electrode weightings for the inner ring of stimulus patches near the fovea while the top row is for the outermost eccentric ring. The 24 topographies in each row reflect the stimulus patch positions going clockwise from the patch just past 12 o'clock to the patch just before 12 o'clock. Keep in mind the 96 electrodes (small dots in the figure) for the individual patch topographies are primarily over the occipital pole. In each topography the position of theinion is just below the lowest electrode and the vertex is only about 3 electrodes positions below the highest electrode position. The most important features to note from this collection of electrode weightings are regions of very similar topographies that change gradually and regions of abrupt topography changes which presumably reflect rapid changes in the cortical surface normal as the cortical region of activation enters the base or apex of a cortical sulcus or gyrus, respectively. It is this association of sparse rapid changes in response topography and the corresponding scarce cortical folding that will enable us to accurately localize the signal sources.

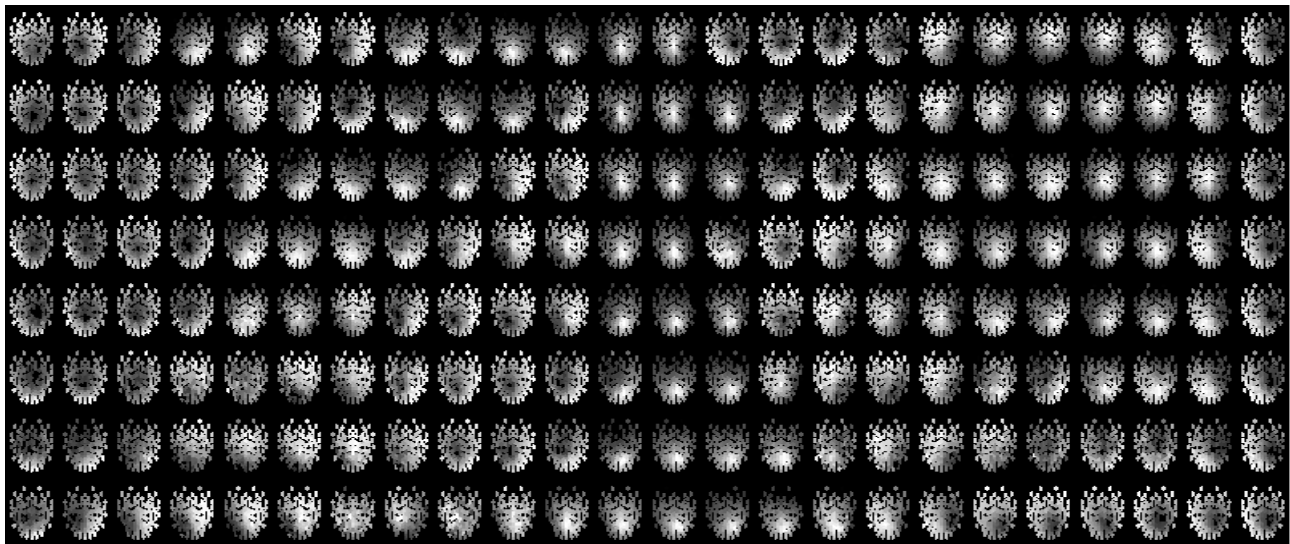


Figure 9 - First component scalp topographies for the 192 patch stimulus.

The surface topographies shown in figure 9 are very similar to surface topographies derived from the adjacent patch cross kernels described earlier. The similarity is to be expected since we believe the cross kernels reflect cortical activation of the area boarding adjacent patches and consequently should have similar topographies. To examine this issue further we have developed a dense VEP based map of V1 surface normals based on interleaving both the self kernel and cross kernel responses. A plot about 400 hundred scalp topographies is perceptually daunting, so each topography was simplified by a vector representing a cortical surface normal that would generate the scalp topography.

A four shell dipole source analysis was used to estimate an equivalent dipole source for each of the self and cross kernel (192 x 2) scalp topographies. To a first approximation the dipole locations are reasonable in that upper and lower, left and right stimulus patches have source solutions that correspond to appropriate hemispheres and lower and upper positions within early visual cortex. However, since we know simple DSL is prone to error, for the presentation in Fig. 10 we fixed the dipole sources to have the same cortical location for a given hemifield. With a cortical location in the middle of V1, the <2 cm location errors would have little impact on the source orientation (our estimate of the cortical surface normal) which is the important parameter that we are estimating. Figure 10 shows the dipole source orientation and magnitudes for the left (panel a) and right hemispheres (panel b). The sources for each hemisphere are plotted, in an 8 by 23 rectangular grid corresponding to the 8 rings of 12 stimulus patches within a visual hemifield. The ring near the fovea is again the bottom row of each plot and the most eccentric ring is the top row of each plot. Each row contains 23 surface normal estimates, 12 from the self kernels (circular lollipop) interleaved with 11 from the adjacent patch cross kernels (triangular lollipop). Each patch source vector is depicted by a lollipop shaped icon where the diameter of the circular base indicates signal strength and filled or open base indicates the vector pointing below or

above the plane. The lollipop handle indicates the source direction as viewed from above the plane such that a very short handle slightly to the left indicates a source point slightly to the left but nearly straight towards the observer. A long lollipop handle pointing to the right indicates a source that is pointing to the right and is nearly in the plane and so for all the pictured sources. Regions of consistent source orientation and transition patches to different orientation are evident as expected for a surface normal representation of a sparsely folded cortical surface. Also note that the orientation of the cross kernel derived sources (triangular lollipops) are generally very similar to the adjacent sources (circular lollipops) which are derived from the patch self kernels. Aligning this VEP based surface normal map with a surface normal map of V1 derived from an MRI scan from the same subject should provide an accurate localization of each of the patch sources.

The separation between lollipops in the tangential direction is about 1.8 mm in V1 for eccentricities greater than about 2 degrees, and down to about 1 mm at smaller eccentricities. The width of V1 for eccentricities greater than 2 deg is about 45 mm based on fMRI/MRI measurements of the brain shown in Fig. 10, in going from the upper to lower vertical meridian. This brain size was close to the mean values reported by Dougherty¹⁴ and Shira¹². For lower eccentricities it can be less than half that amount. Since there are 27 interleaved self- and cross- kernel topographies the spacing between sources is $45/27 = 1.8$ mm for eccentricities above about 2 deg. This calculation gives this same result as a calculation based on Dougherty's finding of a cortical magnification of 3.3 mm/deg at an eccentricity of 5 deg.

The rotation problem: As stated earlier, a more accurate area V1 time function may actually be comprised of a linear combination of the first two SVD time components. This is known as the rotation problem where the correct time function ($T(t)$) is a rotation between the first two components¹⁵:

$$T_{V1}(t) = T_1(t) \cos(\alpha) + T_2(t) \sin(\alpha) \tag{2a}$$

$$T_{V2}(t) = T_1(t) \cos(\beta) + T_2(t) \sin(\beta) \tag{2b}$$

where α and β are the rotation angles for the true sources. A change in the relative contribution of the first two components are also reflected in a change in the scalp electrode weightings ($E(e,p)$) such that,

$$E_{V1}(e,p) = E_1(e,p) \cos(\beta) - E_2(e,p) \sin(\beta) \tag{3a}$$

$$E_{V2}(e,p) = E_1(e,p) \cos(\alpha) - E_2(e,p) \sin(\alpha) \tag{3b}$$

Different rotation angles, going from 0 to pi, will generate different scalp topographies ranging from the pure first SVD component topographies as shown in figure 9 to a topography reflecting just the second component. Each rotation angle

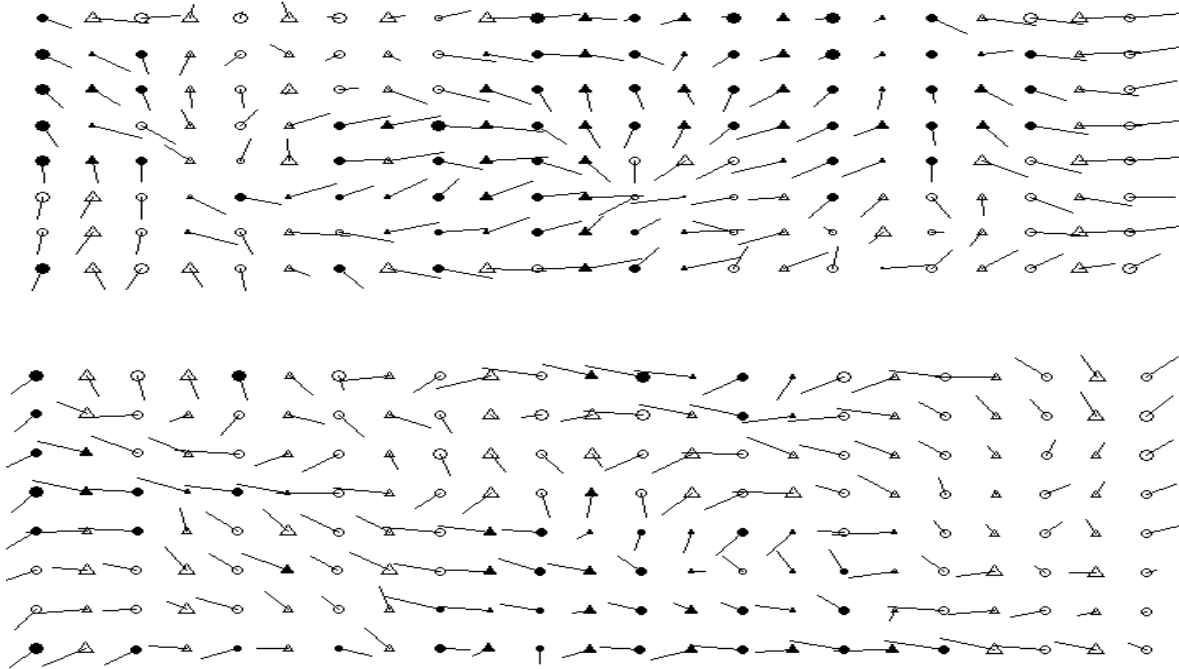


Figure 10 – Hemisphere source orientations for self kernels interleaved with cross kernels: a) left b) right

will consequently generate slightly different source orientation plots from that shown in figure 10 which is for first component alone. The solution of the rotation problem will be given by the best fit between VEP generated cortical source normals and those derived from MRI scans. While the first component may already be the best rotation angle, a small contribution from the second component could improve the fit and reveal a better estimate of the true V1 time component. Moreover, this new rotation would also improve our estimate of the V2 time function.

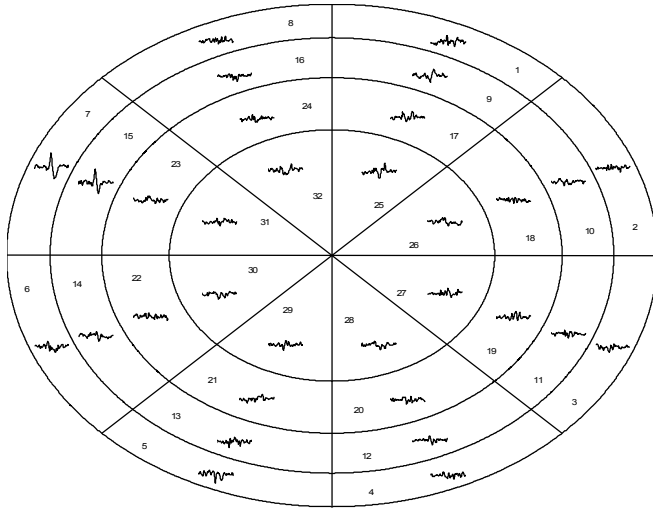


Figure 11 – Response to facial areas

3.2 Extending the multi-focal method to arbitrary grayscale images

Figure 11 shows the responses to the Einstein stimulus shown in Fig. 3, recorded from an electrode located near the vertex, to all 32 stimulus patches. Patches 7 & 15 near Einstein’s right eye evoked the strongest response. This response focus may reflect interesting image content or perhaps a low level stimulus attribute such as an area with greatest mean luminance change. Moreover, the scalp topography appeared to emphasize more frontal areas as compared to the standard checkerboard pattern patches. Much additional research will be needed to answer such questions; the goal here is just to demonstrate the feasibility of using arbitrary grayscale images within the multifocal framework.

3.3 Extracting signals from different neural populations at the same stimulus patch location

The visual cortex is organized into modules or hypercolumns of cells organized along various stimulus dimensions such as orientation and ocular dominance. Within each hypercolumn the response fields of all the cells are positioned in approximately the same location in visual space. Using this same sprite methodology it should be possible to preferentially stimulate different cell populations by manipulating stimulus parameters. For example, the median orientation bandwidth of cells in primate V1 is about 24 degrees, with large individual and cortical cell layer differences

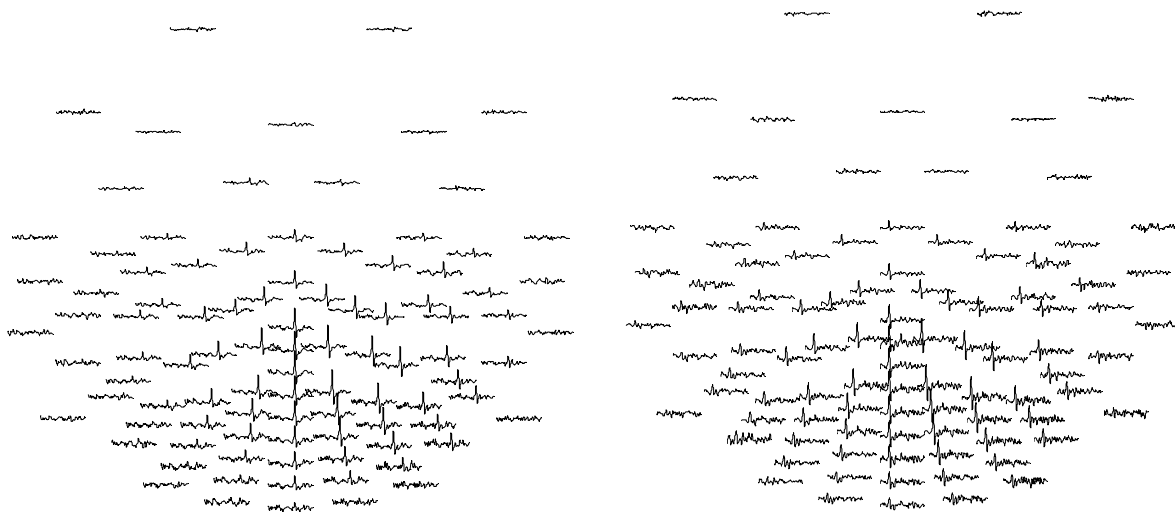


Figure 12 - Tangent and radial grating conditions

including some cells not orientation tuned¹⁶. If two grating stimuli are presented which differ by 90 degrees they should for the most part activate distinct cell populations. Different stimulus configurations could be used to study neural population interactions at discrete spatial locations. This first study included three multi-focal stimulus conditions, The response across electrodes to patch 8 for the tangential and radial grating conditions are shown in figure 12. The radial grating condition (left side of figure) responses appear to be delayed relative to the tangent grating condition (right side of figure). The delay of 400 msec was actually intentionally introduced into the extracted kernels as will become clearer in a moment. In general the response to either type of grating pattern appears roughly the same, which is not unexpected. The interesting condition is the responses shown in figure 13, which is for the multi-pattern multi-focal condition where each stimulus patch contained two independent patterns both of which were temporally modulated by the same m-sequence except for a temporal shift, 400 msec in this particular example. At each electrode position we see two distinct response peaks shifted by 400 msec. Patterns shifted by a particular m-sequence delay show up in the response kernel space with the same delay. If we maximize the kernel (including cross kernel) separation across patches then small patch pattern shifts will also be optimally separated. To examine whether the dual pattern run responses are similar to the two conditions with single patch patterns, we added the separate tangent and radial grating condition kernels, with a 400 msec shift, and compared the sum with the dual pattern condition using SVD as described earlier. Figure 14 shows that the first two time components for the experiment with multiple patterns per stimulus patch actually accounts for more of the variance than the summed results for two independent experiments even though the total recording time was longer for the single pattern conditions. Multiple patterns within a patch also enables extraction of cross pattern kernels to study pattern interactions. Finally, figure 15 compares the time functions for the first component for the multi-pattern experiment with the sum of the two single pattern experiments. In the region of strong signal the two time functions are nearly identical, providing evidence that overlapping multiple conditions in a single experiment can work.

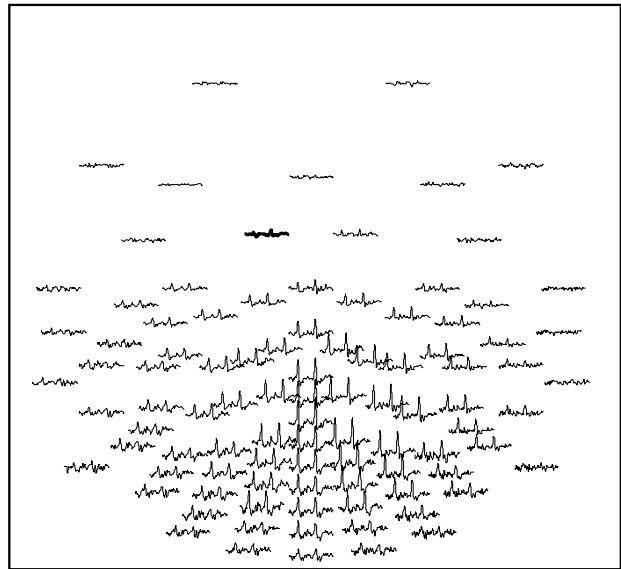


Figure 13 - Multi-pattern multi-focal tangent plus radial grating condition

Figure 14 shows that the first two time components for the experiment with multiple patterns per stimulus patch actually accounts for more of the variance than the summed results for two independent experiments even though the total recording time was longer for the single pattern conditions. Multiple patterns within a patch also enables extraction of cross pattern kernels to study pattern interactions. Finally, figure 15 compares the time functions for the first component for the multi-pattern experiment with the sum of the two single pattern experiments. In the region of strong signal the two time functions are nearly identical, providing evidence that overlapping multiple conditions in a single experiment can work.

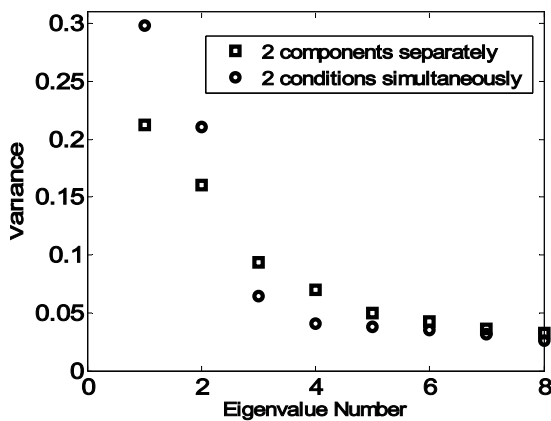


Figure 14 – Comparing single and multi-pattern results

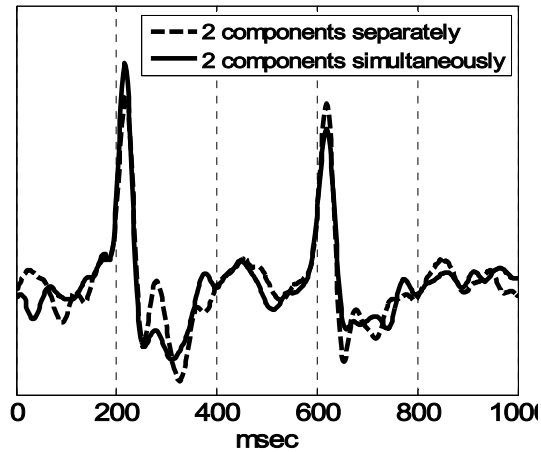


Figure 15 – Comparison of single multi-pattern runs

4. DISCUSSION

The standard multi-focal m-sequence method is a powerful tool to study retinal as well as cortical areas that are retinotopically organized. However the standard implementation based on LUT animation has significant limitations in term of stimulus complexity and stimulus patch density. By using a sprite graphics technique we have been able to overcome such limitations and have recorded VEP responses from targets with hundreds of stimulus patches. With such dense patch arrays and applying cross kernel techniques we recorded responses from areas of cortical activation estimated to be 3.5 x 3.6 mm in size and sampled every 1.8 mm along the cortex of V1 along the direction corresponding to changes in the tangential direction of the stimulus. This dense sampling of visual space with very small stimulus patches provides a detailed map of the local cortical surface normal that can be compared with surface normals derived from MRI scans from the same individual. Not only will we now be able to accurately localize signal sources but we will be able to extract the unique temporal waveforms for the individual early visual areas of the human brain.

Finally, using graphic sprites individual patches can contain multiple arbitrary gray scale images each independently modulated by the same m-sequence but shifted in time. These new multi-pattern multifocal stimuli enable the simultaneous study of local cell populations that differ in sensitivity along stimulus dimensions such as orientation, spatial frequency, color and binocularity while also simultaneously mapping the visual field along those same stimulus dimensions. While we have been applying these new techniques to EEG recordings, the same principals could theoretically be applied to MEG, fMRI and ERG recordings with similar success.

The brain imaging field is on the verge of realizing the long held goal of extracting retinotopically specific information with millisecond temporal resolution. With these advances the temporal dynamics of visual processing in retinotopic visual areas will be accessible to answer questions about cortical processes such as visual attention and awareness.

5. ACKNOWLEDGEMENTS

We wish to acknowledge the contribution of Thang Duong to software development and fruitful ideas for improving reducing kernel overlap and John Torous for improving the plotting algorithms. The research was supported by NEI grant R21

6. REFERENCES

1. Shimada, Y., Li, Y., Bearnse, M.A., Sutter, E.E., Fung, W., "Assessment of early retinal changes in diabetes using a new multifocal ERG protocol", *Br. J. Ophthalmology*, **85**, 414-419, 2001.
2. Slotnick, S.D., Klein, S.A., Carney, T., Sutter, E. & Dastmalchi, S., "Using multi-stimulus VEP source localization to obtain a retinotopic map of human primary visual cortex", *Clinical Neurophysiology*, **110**, 1793-1800, 1999.
3. Slotnick, S.D., Klein, S.A., Carney, T. & Sutter, E.E., "Electrophysiological estimate of human cortical magnification", *Clinical Neurophysiology*, **112**, 4113-4125, 2001.
4. Baseler, H.A., & Sutter, E.E., "M and P components of the VEP and their visual field distribution", *Vision Research*, **37**, 675-690, 1997.
5. Wilhelm, H., Neitzel, J., Wilhelm, B., Beuel, S., Ludtke, H., Kretschmann, U., & Zrenner, E., "Pupil perimetry using m-sequence stimulation technique", *Investigative Ophthalmology and Visual Science*, **41**, 1229-1238, 2000.
6. Vanni, S., Henriksson, L., & James, A.C., "Multifocal fMRI mapping of visual cortical areas", *Neuroimage*, **27**, 95-105, 2005.
7. James, A.C., Ruseckaite, R. & Maddess, T., "Effect of temporal sparseness and dichoptic presentation on multifocal visual evoked potentials", *Visual Neuroscience*, **22**, 45-54, 2005.

8. Baseler, H. A., Sutter, E.E., Klein, S.A. & Carney, T., "The topography of visual evoked response properties across the visual field", *Electroencephalography and Clinical Neurophysiology*, **90**, 65-81, 1994.
9. Sutter, E.E. "A deterministic approach to nonlinear systems analysis", *Nonlinear Vision* (pp. 171-220) New York, CRC Press, 1992.
10. Sutter, E.E., "The fast m-transform: A fast computation of cross-correlations with binary m-sequences", *SIAM Journal for Computing*, **20**, 686-694, 1991.
11. Sutter, E.E. "Imaging visual function with the multifocal m-sequence technique", *Vision Research*, **41**, 1241-1255, 2001.
12. Schira, M.M., Wade, A. R., Kontsevich, L.L., & Tyler, C.W. "Geometric and metric properties of visual areas V1 and V2 in humans", *Journal of Vision*, **5**(8), 897a, 2005.
13. Zhang, X., & Hood, D.C., "A principal component analysis of multifocal pattern reversal VEP", *Journal of Vision*, **4**, 32-43, 2004.
14. Dougherty, R.F., Koch, V.M., Brewer, A.A., Fischer, B., Modersitzki, J. & Wandell, B.A., "Visual field representations and locations of visual areas V1/2/3 in human visual cortex", *Journal of Vision*, **3**, 586-598, 2003.
15. Klein, S.A. & Carney, T. "The usefulness of the Laplacian in PCA and dipole source localization", *Brain Topography Journal of Functional Neurophysiology*, **8**, 91-107, 1995.
16. Ringach, D.L., Shapley, R.M. & Hawken, M.J., "Orientation selectivity in Macaque V1: diversity and laminar dependence", *Journal of Neuroscience*, **22**, 5639-5651, 2002.

* thom@neurometrics.com; phone 510-643-7571; Neurometrics.com